2-1-2006

Fire properties of styrenic polymer–clay nanocomposites based on an oligomerically-modified clay

Jinguo Zhang
Marquette University

David D. Jiang
Marquette University

Charles A. Wilkie
Marquette University, charles.wilkie@marquette.edu

Accepted version. *Polymer Degradation and Stability*, Vol. 91, No. 2 (February 2006): 358-366. DOI.

Polymer Degradation and Stability, Vol. 91, No. 2 (February 2006): 358-366. DOI.

Fire Properties of Styrenic Polymer–Clay Nanocomposites Based on An Oligomerically-Modified Clay

Jinguo Zhang
Department of Chemistry, Marquette University, Milwaukee, WI
David D. Jiang
Department of Chemistry, Marquette University, Milwaukee, WI
Charles A. Wilkie
Department of Chemistry, Marquette University, Milwaukee, WI

Abstract

An oligomerically-modified clay has been used to fabricate nanocomposites with styrenic polymers, such as polystyrene, high-impacted polystyrene, poly(styrene-*co*-acrylonitrile) and acrylonitrile–butadiene–styrene by melt blending. The clay dispersion was evaluated by X-ray diffraction and bright field transmission electron microscopy. All of the nanocomposites have a mixed delaminated/intercalated structure. The fire properties of nanocomposites were evaluated by cone calorimetry a nd the mechanical properties were also evaluated.

Keywords

Nanocomposites, Fire retardancy, Oligomerically-modified clays, Styrenics

1. Introduction

Polymer–clay nanocomposites are very attractive due to the fact that small amount of clay can lead to great improvement in many properties, such as barrier, fire and mechanical, of the polymer [1]. There are two methods commonly used to make polymer–clay nanocomposite: in situ polymerisation and melt blending, and the latter is the preferred method for industry. Since the natural clay is hydrophilic, it typically must be modified by ion exchange with some 'onium' salt before melt blending with the polymer. It is known that to make a polystyrene nanocomposite by melt blending, the clay has to be modified by the onium salt containing two long chains [2], [3], however, one long chain is sufficient for bulk polymerisation.

Previous work from this laboratory has introduced oligomerically-modified clays, which can be used to produce nanocomposites of a variety of polymers by melt blending [4], [5]. More recently, additional oligomerically-modified clays, including those based on butadiene [6] and lauryl acrylate [7] have been introduced. A very interesting new oligomeric clay that has been described contains lauryl acrylate, vinylbenzyl chloride and styrene, and this gives excellent reductions in the peak heat release rate [8]. Because of the presence of styrene in the oligomer, one might expect that this oligomerically-modified clay would be compatible with styrenic polymers, such as polystyrene (PS), high-impact polystyrene (HIPS), poly(styrene-*co*-acrylonitrile) (SAN) and acrylonitrile–butadiene–styrene (ABS).

In this paper, four different styrenic polymers: PS, HIPS, SAN and ABS were melt blended with clay at various clay loading using a Brabender mixer. The morphology of the systems is well-characterized and the fire properties are also examined. The reduction in the peak heat release rate is comparable to those values that have been reported with other clays [9], [10], [11], [12].

2. Experimental

2.1. Materials

Polystyrene (melt index 200 °C/5.0 kg, 7.50 g/10 min) was acquired from the Aldrich Chemical Company, acrylonitrile–butadiene–styrene copolymer (ABS) (melt index 230 °C/3.8 kg, 2.6 g/10 min) and high-impact polystyrene (HIPS) (STYRON 478) were acquired from the Dow Chemical Company. Styrene–acrylonitrile copolymer (SAN) was provided by Cheil Industries Inc. The clay, known as triclay, used in these studies was prepared following the literature procedures [8]. Triclay is composed of three monomers, styrene, vinylbenzyl chloride and lauryl acrylate, with the benzyl unit quaternised and this ammonium salt used for ion exchange with the clay. The complete description of its synthesis and its structure are available [8].

2.2. Preparation of the polymer–clay nanocomposites

Four different polymers, PS, HIPS, SAN and ABS, were combined with the clay at various clay loading. All nanocomposites were prepared by melt blending in a Brabender Plasticorder at 60 rpm and 185 °C for 3 min. The calculated amount of polymer and clay was placed in the Brabender at the same time. After 3 min blending, the mixture was removed from the chamber and allowed to cool to room temperate. Table 1 gives the composition of the nanocomposites that have been prepared and studied.

Table 1. Composition of polymer clay nanocomposites

No.	Polymer	Triclay	Inorganic clay loading (%)
1	96	4	1
2	88	12	3
3	80	20	5

2.3. Instrumentation

X-ray diffraction (XRD) was performed on a Rigaku Geiger Flex, 2-circle powder diffractometer equipped with Cu-Kα generator (λ = 1.5404 Å) at 50 kV and 20 mA, scanning from 1 to 10° in 0.1 steps. All the samples were compression moulded into 20 mm × 15 mm × 1 mm plaques for XRD measurements. Bright field transmission

electron microscopy (TEM) image was obtained at 120 kV, under low-dose conditions, with a Phillips 400T electron microscopy. The sample was ultramicrotomed with a diamond knife on a Leica Ultracur UCT microtome at room temperature to give 70-nm-thick section. The section was transferred from water to carbon-coated Cu grids of 200 mesh. The contrast between the layered silicate and the polymer phase was sufficient for imaging, so no heavy metal staining of sections prior to imaging was required. Thermogravimetric analysis (TGA) was carried out on a Cahn TG131 unit under nitrogen at a scan rate of 20 °C/min from room temperature to 600 °C. Temperatures are reproducible to ±3 °C while the fraction of non-volatile is repeatable to ±3%. Cone calorimetry was performed on an Atlas CONE-2 according to ASTM E 1354 at an incident flux of 35 kW/m^2 using a cone shaped heater. Exhaust flow was set at 24 L/s and the spark was continuous until the sample ignited. Cone samples were prepared by compression molding the composites into 100 mm × 100 mm × 3 mm square plaques. Typical results from cone calorimetry are reproducible to within about ±10%. These uncertainties are based on many runs in which thousands of samples have been combusted [13]. Tensile properties were measured using MTS Alliance RT/5 tensile test machine at a crosshead speed of 5 mm/min. The reported values are based on the average of 5 determinations.

3. Results and discussion

3.1. XRD measurements on the nanocomposites

The clay dispersion in the polymer matrix was evaluated using X-ray diffraction (XRD). The XRD patterns are shown in Fig. 1, Fig. 2, Fig. 3, Fig. 4. For the PS system, the peak position is the same as that seen in the clay itself. This is not unusual and has been observed for polyolefin samples made with triclay [8]. While one might take this as indicating that polymer does not penetrate the gallery space, an alternate explanation is that the gallery space has already expanded sufficiently to permit the entry of additional material without additional expansion. The d-spacing of triclay itself is 3.7 nm, which is large enough to permit the entry of polymer. For the HIPS system, with 4% triclay in the HIPS composite, a peak appears at 1.2°, possibly indicating that some HIPS chains have intercalated. At higher clay loadings, 12% and 20%, a broad feature, not a sharp peak, appears around 1.2°. For the SAN system, a peak cannot be seen at any clay loading, but there is a widening of the curve at higher clay loadings, which could mean that delamination has occurred. For the ABS system, there is a new peak at 1.4° for 4% triclay loading, but this is absent at higher clay loadings but a broad feature appears in the 2° region; this could be an indication of disorder in this system. XRD gives an indication of the type of hybrid that has been produced but transmission electron microscopy is required to image the clay platelets and fully identify the type of nanocomposite that has been produced.

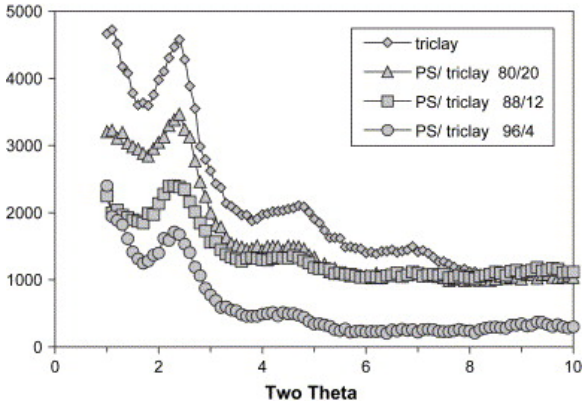

Fig. 1. X-ray diffraction pattern of PS/triclay nanocomposites.

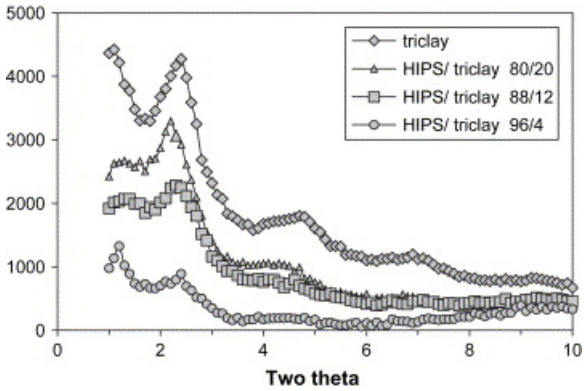

Fig. 2. X-ray diffraction pattern of HIPS/triclay nanocomposites.

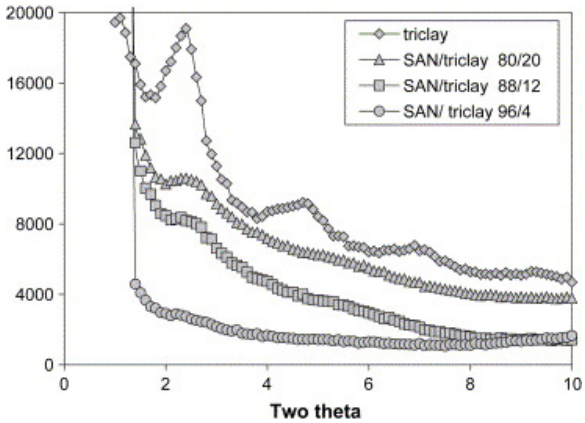

Fig. 3. X-ray diffraction pattern of SAN/triclay nanocomposites.

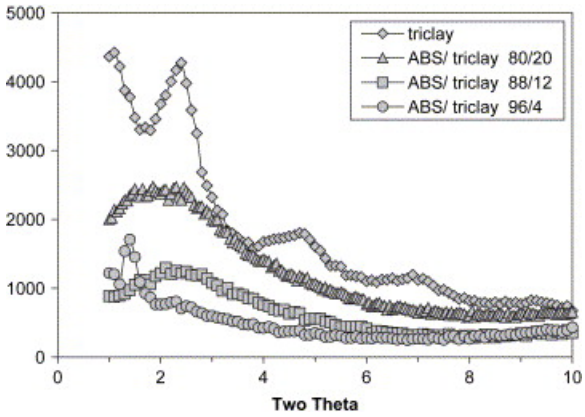

Fig. 4. X-ray diffraction pattern of ABS/triclay nanocomposites.

3.2. Transmission electron microscopy (TEM) measurements on the nanocomposites

TEM images were obtained for the PS, HIPS, SAN and ABS nanocomposites with 5% inorganic clay loading. The TEM images are shown in Fig. 5, Fig. 6, Fig. 7, Fig. 8. From the low magnification TEM images, one can clearly see that the clay is well-distributed throughout the polymer matrix. From the high magnification TEM images, single layers combined with some tactoids are evident in all systems. The TEM images for the ABS system appears a bit coarser than the other systems. From the XRD and the TEM results, one can conclude that the nanocomposites have a mixed morphology, containing both delaminated and intercalated structures.

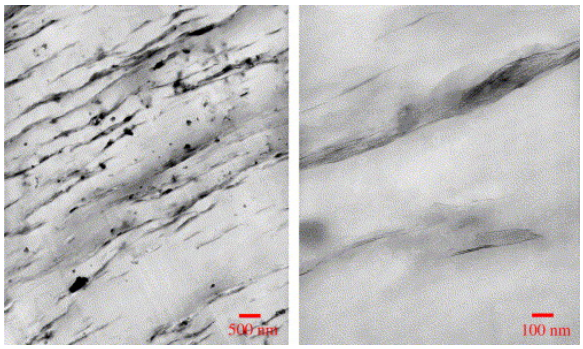

Fig. 5. TEM images of PS/triclay nanocomposite at 5% inorganic clay loading.

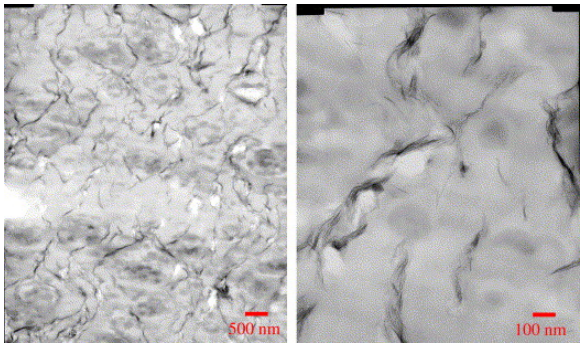

Fig. 6. TEM images of HIPS/triclay nanocomposite at 5% inorganic clay loading.

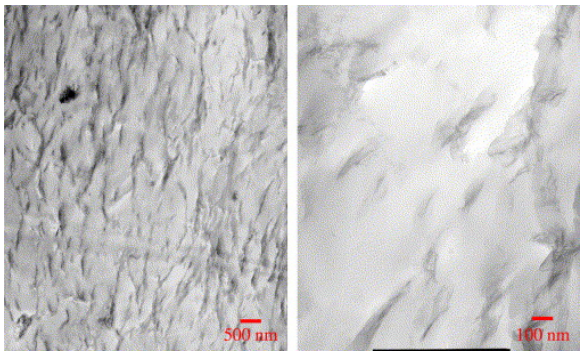

Fig. 7. TEM images of SAN/triclay nanocomposite at 5% inorganic clay loading.

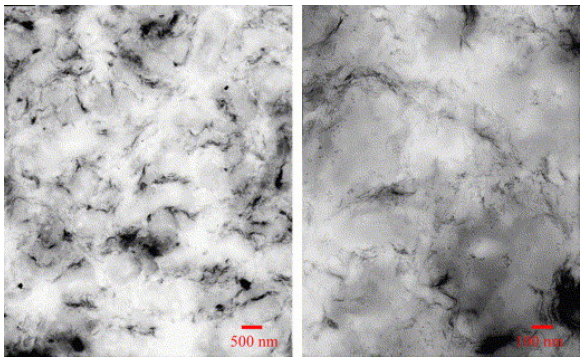

Fig. 8. TEM images of ABS/triclay nanocomposite at 5% inorganic clay loading.

3.3. TGA characterization of the nanocomposites

The thermal degradation behaviour of the pure polymers and their triclay nanocomposites was measured by thermogravimetric analysis (TGA). The parameters that are of interest from the TGA curves are the onset of the degradation, which is usually taken as the temperature at which 10% degradation occurs, $T_{0.1}$, the mid-point temperature of the degradation, $T_{0.5}$, another measure of thermal stability, and the non-volatile residue which

remains at 600 °C, denoted as char. The data are tabulated in Table 2, Table 3, Table 4, Table 5 and are also shown graphically in Fig. 9, Fig. 10, Fig. 11, Fig. 12. For the PS nanocomposites, the changes in $T_{0.1}$ with 1% and 3% inorganic clay loading are within experimental error, while $T_{0.1}$ has a 7 °C decrease with 5% inorganic loading compared to virgin PS. For the HIPS, SAN and ABS systems, the onset degradation temperature decreases, which may be due to the presence of the oligomer. This should be contrasted to the behaviour of other oligomerically-modified clays that have been previously reported. For styrene nanocomposites, the temperature at which 10% degradation occurs increases by 25 °C for the styryl-modified clay [4], the caprolactone-modified clay [10] and the butadiene-modified clay [6]. The onset of the degradation of HIPS either decreases or shows no change with all oligomerically-modified clays that have been studied in this laboratory. Finally, For ABS, in some cases there is a decrease while in others, caprolactone and butadiene, there is an increase. There is a significant difference between triclay and the other oligomerically-modified clays that have been studied in that triclay begins to degrade much earlier than do the others. Thus the likely explanation for the lower onset temperatures is the instability of the triclay. Considering the difference in thermal stability, it is surprising how great is the thermal stability exhibited by these nanocomposites.

Table 2. TGA data, in nitrogen, for PS/triclay nanocomposites

PS	Triclay	$T_{0.1}$	$T_{0.5}$	Char (%) at 600 °C
100	–	417	447	0
96	4	418	456	2
88	12	420	470	5
80	20	410	470	7
–	100	370	427	25

Table 3. TGA data, in nitrogen, for HIPS/triclay nanocomposites

HIPS	Triclay	$T_{0.1}$	$T_{0.5}$	Char (%) at 600 °C
100	–	440	464	0
96	4	440	473	3
88	12	425	474	5
80	20	425	476	6
–	100	370	427	25

Table 4. TGA data, in nitrogen, for SAN/triclay nanocomposites

SAN	Triclay	$T_{0.1}$	$T_{0.5}$	Char (%) at 600 °C
100	–	424	452	1
96	4	424	443	3
88	12	414	450	6
80	20	413	453	8
–	100	370	427	25

Table 5. TGA data, in nitrogen, for ABS/triclay nanocomposites

ABS	Triclay	$T_{0.1}$	$T_{0.5}$	Char (%) at 600 °C
100	–	430	455	1
96	4	428	463	3
88	12	425	465	6
80	20	420	462	8
–	triclay	370	427	25

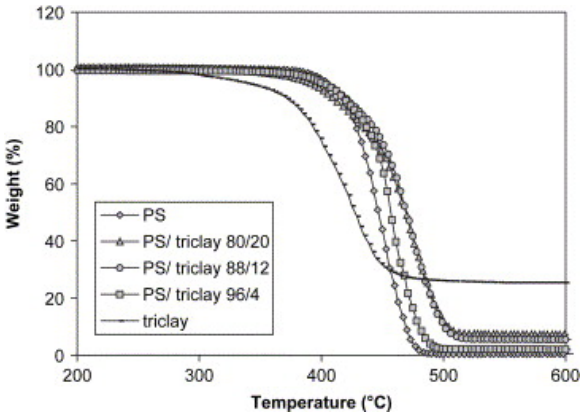

Fig. 9. TGA curves for PS/triclay nanocomposites.

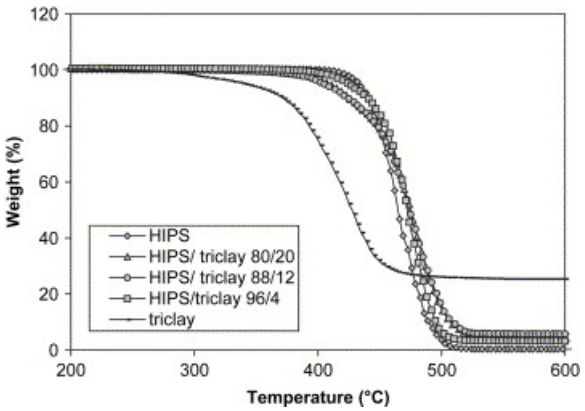

Fig. 10. TGA curves for HIPS/triclay nanocomposites.

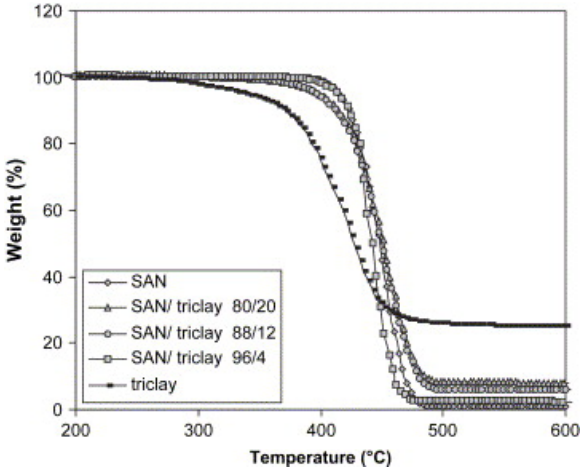

Fig. 11. TGA curves for SAN/triclay nanocomposites.

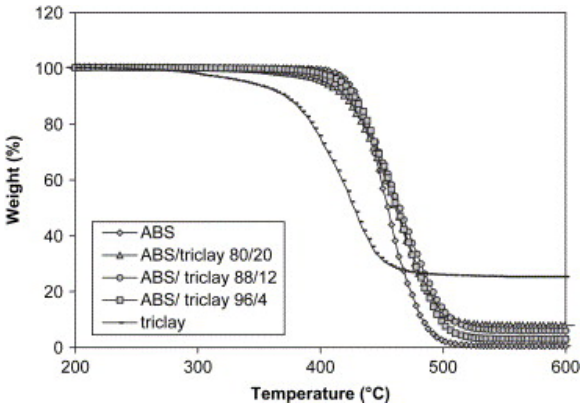

Fig. 12. TGA curves for ABS/triclay nanocomposites.

There is some enhancement for $T_{0.5}$ in all nanocomposites except SAN nanocomposites even though the $T_{0.5}$ of triclay is 20–30 °C lower than that of the pure polymers. PS nanocomposites show the greatest improvement, increasing by 23 °C with 3% and 5% inorganic clay loading. HIPS nanocomposite shows a 12 °C increase with 5% inorganic clay loading, and ABS nanocomposite shows a 7 °C increase. With most of the other oligomerically-modified clays, $T_{0.5}$ increases by 5–30 °C. All of the improvement for $T_{0.5}$ may be attributed to a nanocomposite effect. The char formed at 600 °C is slightly greater than the amount of inorganic clay that has been added, but most of the increases are within experimental error.

3.4. Fire properties of the nanocomposites

The fire properties of materials were evaluated by cone calorimeter. The parameters that are evaluated include the time to ignition (t_{ign}); the heat release rate, and especially its peak value, (PHRR); the total heat released (THR), a measure of how much of the polymer actually undergoes combustion; the specific extinction area (SEA), a measure of the amount of smoke produced during the combustion; and the mass loss rate (MLR). Cone calorimeter also provides useful information on nanocomposite formation, since it has been shown that microcomposites give essentially no reduction in the peak heat release rate, while nanocomposites can give significant reductions [14], [15].

The cone calorimetric results for the various nanocomposites are shown in Table 6, Table 7, Table 8, Table 9 and the heat release rate curves for the pure polymer and its nanocomposites are shown graphically in Fig. 13, Fig. 14, Fig. 15, Fig. 16. The PHRR of PS nanocomposites show a maximum 60% reduction compared with virgin PS. The PHRR of HIPS nanocomposites show a maximum 50% reduction compared with virgin HIPS, while SAN nanocomposites show a maximum 40% reduction compared with virgin SAN and ABS nanocomposites show a maximum 35% reduction compared with virgin ABS. These values are comparable to the best reductions that have been obtained for these various polymers [9], [10], [11], [12]. The total heat released is essentially unchanged, which is what is normally observed for nanocomposites and indicates that everything does eventually burn. The SEA value gradually increases as the amount of clay increases, indicating that clay in the system can lead to more smoke. The maximum decrease in the mass loss rates for PS, HIPS, SAN and ABS are 60%, 50%, 40% and 30%, respectively, the same trend as PHRR reduction. Since the reduction in PHRR follows the reduction in mass loss rate, this correlation is essential to observe.

Table 6. Cone calorimetric data for PS and its triclay nanocomposites 35 kW/m^2

PS	Triclay	t_{ign} (s)	PHRR (kW/m^2) (% reduction)	SEA (m^2/kg)	MLR (g/s m^2)	THR (MJ/m^2)
100	0	64 ± 2	1328 ± (34)	1124 ± 27	35 ± 0	86 ± 1
96	4	54 ± 3	1070 ± 53 (19)	1117 ± 24	29 ± 1	80 ± 4
88	12	46 ± 1	699 ± 21 (47)	1259 ± 27	19 ± 1	84 ± 1
80	20	42 ± 1	521 ± 4 (61)	1323 ± 11	14 ± 0	81 ± 3

t_{ign}, Time to ignition; PHRR, peak heat release rate; % reduction = $PHRR_{PS} - PHRR_{nano}/PHRR_{PS}$; SEA, specific extinction area; MLR, mass loss rate; THR, total heat released.

Table 7. Cone calorimetric data for HIPS and its triclay nanocomposites 35 kW/m^2

HIPS	Triclay	t_{ign} (s)	PHRR (kW/m^2) (% reduction)	SEA (m^2/kg)	MLR (g/sm^2)	THR (MJ/m^2)
100	0	72 ± 2	1339 ± 92	1257 ± 38	32 ± 2	102 ± 1
96	4	65 ± 5	1250 ± 27 (7)	1265 ± 10	30 ± 1	95 ± 3
88	12	57 ± 3	756 ± 6 (44)	1405 ± 39	18 ± 0	96 ± 1
80	20	50 ± 2	662 ± 35 (51)	1400 ± 29	16 ± 1	90 ± 3

t_{ign}, Time to ignition; PHRR, peak heat release rate; % reduction = $PHRR_{HIPS} - PHRR_{nano}/PHRR_{HIPS}$; SEA, specific extinction area; MLR, mass loss rate; THR, total heat released.

Table 8. Cone calorimetric data for SAN and its triclay nanocomposites 35 kW/m^2

SAN	Triclay	t_{ign} (s)	PHRR (kW/m^2) (% reduction)	SEA (m^2/kg)	MLR (g/sm^2)	THR (MJ/m^2)
100	0	54 (±4)	1113 (±35)	1132 (±15)	30 (±0)	83 (±2)
96	4	50 (±3)	904 ± 46 (19)	1159 (±12)	26 (±1)	83 (±2)
88	12	47 (±2)	813 ± 19 (27)	1221 (±15)	23 (±0)	88 (±1)
80	20	48 (±2)	650 ± 13 (42)	1291 (±20)	18 (±0)	86 (±0)

t_{ign}, Time to ignition; PHRR, peak heat release rate; % reduction = $PHRR_{SAN} - PHRR_{nano}/PHRR_{SAN}$; SEA, specific extinction area; MLR, mass loss rate; THR, total heat released.

Table 9. Cone calorimetric data for ABS and its triclay nanocomposites 35 kW/m^2

ABS	Triclay	t_{ign} (s)	PHRR (kW/m^2) (% reduction)	SEA (m^2/kg)	MLR (g/sm^2)	THR (MJ/m^2)
100	0	67 ± 6	1110 ± 41	1133 ± 18	28 ± 1	92 ± 3
96	4	55 ± 3	1086 ± 26 (2)	1170 ± 11	27 ± 1	87 ± 1
88	12	58 ± 3	893 ± 37 (20)	1209 ± 18	22 ± 1	86 ± 2
80	20	53 ± 2	724 ± 57 (35)	1228 ± 41	19 ± 1	88 ± 1

t_{ign}, Time to ignition; PHRR, peak heat release rate; % reduction = $PHRR_{ABS} - PHRR_{nano}/PHRR_{ABS}$; SEA, specific extinction area; MLR, mass loss rate; THR, total heat released.

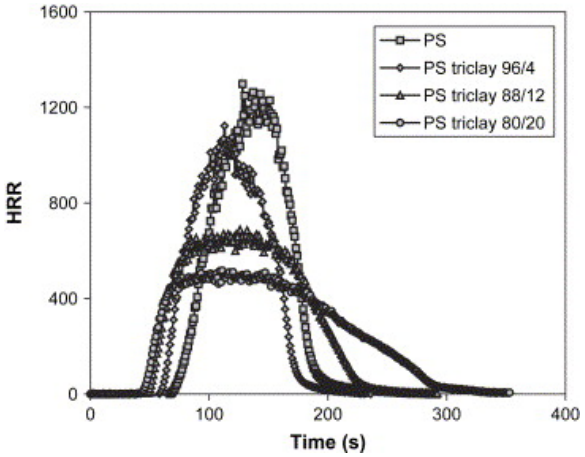

Fig. 13. Comparison of the heat release rate (HRR) plots for pure PS and its nanocomposites at 35 kW/m^{2}heat flux.

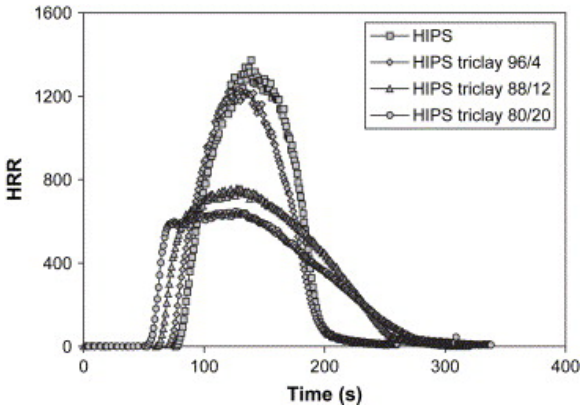

Fig. 14. Comparison of the heat release rate (HRR) plots for HIPS and its nanocomposites at 35 kW/m^2 heat flux.

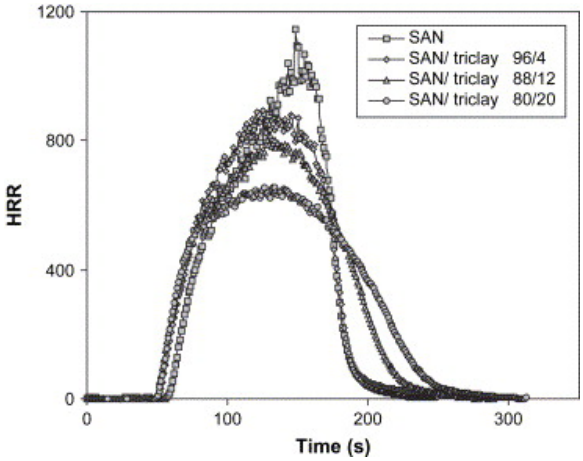

Fig. 15. Comparison of the heat release rate (HRR) plots for SAN and its nanocomposites at 35 kW/m^2 heat flux.

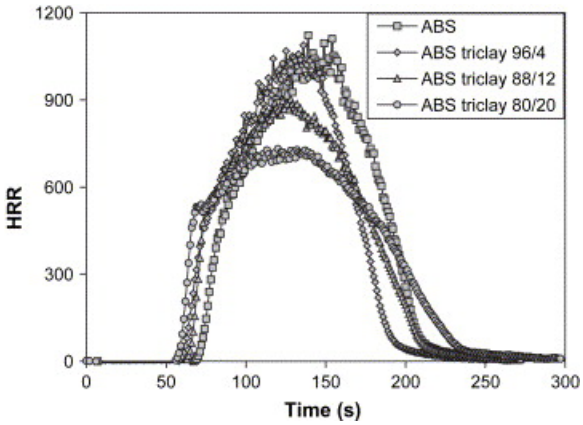

Fig. 16. Comparison of the heat release rate (HRR) plots for ABS and its nanocomposites at 35 kW/m^2 heat flux.

Photographs of the residues from triclay nanocomposites after burning in the cone calorimeter are displayed in Fig. 17. One can clearly see that the small amount of residue covers a very limited space at low clay content (left most image) while a large amount of expanded residue covers most of the space with 12% triclay (3% inorganic clay) present (right most image in each set). At 5% inorganic clay content, a residue that maintains the same shape as before combustion is observed for all four styrenic polymers.

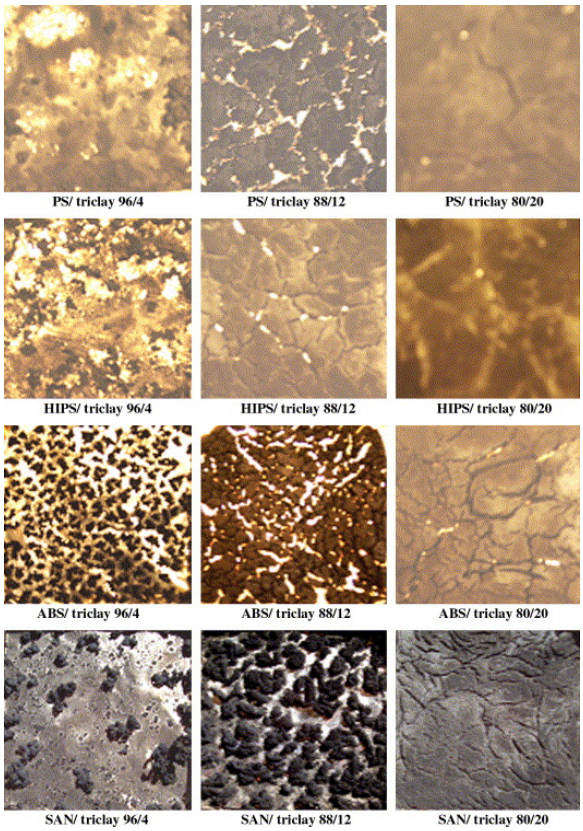

Fig. 17. Photographs of the residues of polymer/triclay nanocomposites after cone calorimetry.

3.5. Mechanical properties

The mechanical properties such as tensile strength, Young's modulus and elongation at break, have been evaluated and the data are tabulated in Table 10. From the data, it is clearly seen that nanocomposite formation does not improve the mechanical properties. In most case, the tensile strength and Young's modulus decrease and elongation also decreases for the HIPS and ABS systems while the change in elongation for PS is within experimental error. The data for SAN system are not available due to the difficulty in making the specimens (Table 10).

Table 10. Tensile properties of polymers and their triclay nanocomposites

	Triclay	**Tensile strength (MPa)**	**Young's modulus (MPa)**	**Elongation at break (%)**
PS				
100	0	30	1574	2
96	4	26	1413	3
88	12	24	996	3
80	20	21	855	3
HIPS				
100	0	18	1032	30
96	4	18	880	28
88	12	16	857	14
80	20	10	510	3
ABS				
100	0	27	790	35
96	4	27	976	13
88	12	26	800	5
80	20	25	876	4

4. Conclusions

PS, HIPS, SAN and ABS nanocomposites have been successfully made by melt blending polymer with an oligmerically-modified clay, “triclay”. The onset temperature of the degradation for the nanocomposites decreases due to the presence of oligmer, but the main degradation temperature increases. All nanocomposites show good reduction in peak heat release rate at 5% inorganic clay loading; these reductions are comparable to the best values that have been obtained for each of these polymeric systems.

References

[1] M. Alexandre, P. Dubois. *Mater Sci Eng*, R28 (2000), pp. 1-63

[2] D. Wang, J. Zhu, Q. Yao, C.A. Wilkie. *Chem Mater*, 14 (2002), pp. 3837-3843

[3] J.W. Gilman, T. Kashiwagi, E.P. Giannelis, E. Manias, S. Lomakin, J.D. Lichtenham, *et al.. Fire Retard Polym*, 224 (1998), pp. 203-221. [Special Publication – Royal Society of Chemistry

[4] S. Su, D.D. Jiang, C.A. Wilkie. *Polym Degrad Stab*, 83 (2004), pp. 333-346

[5] S. Su, D.D. Jiang, C.A. Wilkie. *Polym Degrad Stab*, 83 (2004), pp. 321-331

[6] S. Su, D.D. Jiang, C.A. Wilkie. *Polym Degrad Stab*, 84 (2004), pp. 279-288

[7] J. Zhang, D.D. Jiang, C.A. Wilkie. *Thermochim Acta*, 430 (2005), pp. 107-113

[8] Zhang J, Jiang DD, Wilkie CA. *Polym Degrad Stab*, in press.

[9] J. Zhu, F.M. Uhl, A.B. Morgan, C.A. Wilkie. *Chem Mater*, 13 (2001), pp. 4649-4654

[10] X. Zheng, C.A. Wilkie. *Polym Degrad Stab*, 82 (2003), pp. 441-450

[11] S. Bourbigot, D.L. Vanderhart, J.W. Gilman, S. Bellayer, H. Stretz, D.R. Paul. *Polymer*, 45 (2004), pp. 7627-7638

[12] S. Wang, Y. Hu, Z. Lin, Z. Gui, Z. Wang, Z. Chen, *et al.. Polym Intern*, 52 (2003), pp. 1045-1049

[13]J.W. Gilman, T. Kashiwagi, M. Nyden, J.E.T. Brown, C.L. Jackson, S. Lomakin, *et al.* S. Al-Maliaka, A. Golovoy, C.A. Wilkie (Eds.), *Chemistry and technology of polymer additives*, Blackwell Scientific, London (1998), pp. 249-265

[14] M. Zanetti, G. Camino, D. Canavese, A.B. Morgan, F.J. Lamelas, C.A. Wilkie. *Chem Mater,* 14 (2002), pp. 189-193

[15] J. Zhu, P. Start, K.A. Mauritz, C.A. Wilkie. *Polym Degrad Stab,* 77 (2002), pp. 253-258